RSC Advances

ROYAL SOCIETY OF CHEMISTRY

www.rsc.org/advances

Characterizations of Li-doped WO_3 nanowires and their enhanced electrocatalytic oxidation of ascorbic acid

Wanjun Mu, Xiang Xie, Rui Zhang, Xingliang Li, Kai Lv, Qianhong Yu, Hongyuan Wei[*], *Yuan Jian*

Institute of Nuclear Physics and Chemistry , China Academy of Engineering Physics, 64# Mianshan Road, Mianyang, 621900, Sichuan Province, P. R. China.

Wanjun Mu: Mail address is as above and Email: muwj1012@163.com

Xiang Xie: Mail address is as above and Email: xiexiangster@gmail.com

Rui Zhang: Mail address is as above and Email: 374723080@qq.com

Xingliang Li: Mail address is as above and Email: 84611755@qq.com

Kai Lv: Mail address is as above and Email: muwanjun@163.com

Qianhong Yu: Mail address is as above and Email: yqh2812@163.com

Yuan Jian: Mail address is as above and Email: jianyuanpku@163.com

Hongyuan Wei: Mail address is as above and Email: muwj2014@163.com

[*] Corresponding author: Tel: +86 816 2494854.

E-mail address: muwj2014@163.com

ABSTRACT

Li-doped WO_3 nanowires have been hydrothermally prepared and characterized mainly via spectroscopy methods. Both the hexagonal structure distortion and morphology evolution induced by Li doping reveal a lattice expansion about 0.07Å. Also, the residence of oxygen vacancy, the enlargement of external surface areas positively correlate with the narrowing of energy band. Sequently, the electrocatalytic oxidation of Ascorbic Acid using Li-doped WO_3 film-coated electrode performs a 13%, 21% negative shift of the oxidation overpotential compared with WO_3 film-coated electrode, bare glassy carbon electrode, respectively. A preliminary mechanism has been proposed on the basis of relevant model analyses.

Keywords: Li-doped, tungsten oxide, electrocatalysis, ascorbic acid

1. Introduction

As an indispensable ingesta that participates in many biochemical reactions of human physiology, the detection of Ascorbic Acid (AA) in the circumstance of human body fluid has been of significance in assessing the status of health. Electrochemical sensor adopting a variety of chemical-modified electrode renders a progressive technology of overcoming the disadvantages of high overpotential, poor reproducibility, low selectivity and sensitivity on conventional electrodes.[1-4] Thus, much interest has been focused on the use of mediators and modified electrodes to catalyze the oxidation of AA. [5-6]

It has been well recognized that oxide-based semiconductors display excellent electrocatalytic activity due to their unique phyiscochemical properties.[8-14] However, the concentration of free electrons in metal oxide semiconductors is low i.e., ~10^{21} electrons m^{-3}.[14] A valid approach to enhance the electrocatalytic performance is metal doping that achieves a significant raise in free electron concentration exemplified by Nb-doped TiO_2/carbon composite and Li-doped tantalum oxide, [15-17] wherein the electron conductivity and electrocatalytic activity of both improve.

Tungsten oxide (WO_3) is a versatile wide band gap metal oxide that finds its extensive application as elctrochromic, photochromic, photocatalytic devices.[18-25] Besides, WO_3 can be utilized as electrode modifier attributed to its high chemical stability and considerable semiconductivity. Thus, the electrocatalytic property of WO_3 in the morphology of nanorods, nanowires and its aggregates has been highlighted.[26] Compared with the pristine WO_3, the metal-doped ones can further

improve the electrochemical properties of WO_3. As exemplified, Bathe et al. showed that the cyclic stability, charge storage capacity, and reversibility could be improved by addition of Nb_2O_5 to WO_3 films.[27] Also, Ti-doped WO_3 film can improve their electrical conductivity and reaction kinetics.[28] However, the effect of doping on the electroactivity of WO_3 is rarely studied. We propose that development of highly efficient Li-doped WO_3 electrocatalyst and its application in the electrochemical detection of ascorbic acid in biological systems will be of interest to a broad range of material scientists，as Li ions doping can affects oxygen vacancies, energy band gap and surface area of WO_3.

In our previous work, we successfully prepared Ta-doped tungsten oxide nanowire and studied their electrocatalytic activity for hydrogen evolution reaction.[29] In this paper, Li-doped WO_3 film has been fabricated and homogenously deposited on glassy carbon electrode. A test of its electrocatalytical oxidation of AA has been carried out to investigate the effect of experimental parameters of cyclic voltammetry in order to explore the mechanism.

2. Experimental

2.1. Chemical reagents and synthesis of Li-doped WO_3 nanowires

Sodium tungstate dihydrate ($NaWO_4 \cdot 2H_2O$, analytical grade) was purchased from Kelong Company, lithium nitrate ($LiNO_3$, 99.9%, analytical grade) was purchased from Sigma–Aldrich, ammonium sulfate ($(NH_4)_2SO_4$) was received from Tianjin Chemical Reagents Corporation (China). All other chemicals were purchased from Chengdou Chemical Reagents Corporation (China).

The synthetic method of Li-doped WO_3 is as follows: 2 g of $Na_2WO_4 \cdot 2H_2O$ and $LiNO_3$ (at varying Li / W mole ratios of 0, 0.01, 0.03, 0.05, 0.07, and 0.1) was dissolved in 45 mL deionized water under stirring at room temperature, then 5 mL of 3 mol L^{-1} HCl solution was added to the above solution under continuous stirring until tungstenic acid was heavily precipitated, finally 30 mL of 0.5 mol L^{-1} $(NH_4)_2SO_4$ solution was added to this solution, which was then transferred to a Teflon-lined autoclave with a capacity of 100 mL. Hydrothermal treatments were carried out at 200°C for 24 h. After that, the autoclave was allowed to cool naturally. The final products were collected, washed with deionized water and ethanol several times, and dried in air at 80°C. The Li-doped WO_3 nanowires were finally obtained.

2.2. Characterization of Li-doped WO_3 nanowires

Powder X-ray diffraction (PXRD) analysis was conducted to characterize the crystalline phase of the Li-doped WO_3 samples on a X'Pert PRO PANalytical diffractometer (Almelo, Netherlands) with Cu Kα radiation (λ 0.15406 nm), operating at 40 kV and 45 mA. The size and shape of the samples were observed on a field-emission scanning electron microscope (FESEM, Philips XL30 FEG, Eindhoven, Netherlands) and transmission electron microscope (TEM, JEM200CX, 120 kV). X-ray photoelectron spectroscopy (XPS) was performed on a RBD upgraded PHI-5000C ESCA system (PerkinElmer) using Mg-monochromatic X-ray at a power of 25 W and an X-ray-beam diameter of 10 mm, and a pass energy of 29.35 eV. The binding energy was calibrated using the C1s hydrocarbon peak at 284.8 eV. UV–vis diffuse reflectance spectroscopy was carried out on an UV–vis spectrophotometer

(Lambda 850, PerkinElmer, USA), equipped with an integrating sphere and a $BaSO_4$ reference. Nitrogen adsorption and desorption isotherms were measured at 77 K with a Beckman Coulter SA 3100 surface area analyzer. To determine the surface area, the Brunauer–Emmett–Teller (BET) method was used. The doped amount of lithium in WO_3 was measured with inductive coupled plasma (VISTA-MPX CCD Simultaneous ICP-OES, Varian, USA).

2.3. Electrochemical measurements

The Li-doped WO_3 nanowires were further characterized using cyclic voltammetry (CV) in the 0.1 mol L^{-1} KCl containing 0.4 mmol L^{-1} AA as the electrolyte solution. Prior to the electrochemical measurements, high-purity Ar_2 was bubbled in the above solution for 20 min. During the experiments, high-purity Ar_2 was continually bubbled at the surface of the electrolyte solution. The fabrication of the Li-doped WO_3 film- and pure WO_3 film-coated electrodes is as follows: 20 mg of Li-doped WO_3 or WO_3 powder was dispersed ultrasonically in a mixture of 1.0 mL ethanol and 8 μL nafion solution to obtain a suspension. The suspension was spread on the glassy carbon electrode (GCE), and dried for 10 min at 25°C. This film-coated GCE was used as a working electrode. A Pt coil and an Ag/AgCl electrode (3mol L^{-1} KCl) were used as the counter and reference electrodes, respectively. The CV measurements were carried out on a CHI 660C electrochemical workstation (Shanghai Chenhua Instrument Factory, China) at room temperature (22 ± 2°C).

3. Results and discussion

3.1. Structure and morphology of the pristine and Li-doped WO_3

The XRD patterns of pristine and Li-doped WO_3 presented in Fig.1 demonstrate a hexagonal phase of good crystallinity with lattice constants a = 7.299 Å and c = 3.899 Å (JCPDS Card No. 33-1387). No lithium-bearing impurities have been found and the diffraction peak of (001) facet shifts to lower degree as the lithium doping amount increases. The observations indicate that the lithium ion has been incorporated into the WO_3 lattice and therefore induce local distortions as a result of a slight lattice expansion.

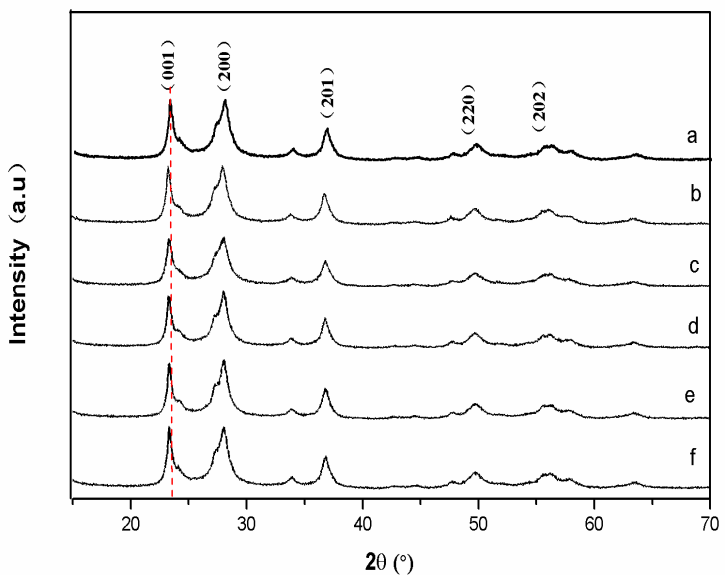

Fig. 1. XRD patterns the Li-doped WO_3 nanowires at varying Li/W molar ratios of (a)–(f) 0, 0.01, 0.03, 0.05, 0.07, and 0.10, respectively.

Both pristine and Li-doped WO_3 illustrated by Fig.2 unfold coral-like tangled nanowires forming accessible hierarchical pores. The diameter of those nanowires is in the range of 20 to 30 nm while the length of Li-doped nanowires is roughly longer than that of the pristine. The high-resolution transmission electron microscopy presented in Fig.2c, f indicated a marked fringe with the spacing of 0.375, 0.382 nm for the pristine and doped, respectively. Since the labeled fringe corresponds to the

(001) facet, the lattice spacing expands 0.07Å according with the XRD analysis results. Both crystal structure and morphology representations imply that a lattice defect induced by the substitution of W^{5+}/W^{6+} with Li^{+} proceeds to cause local lattice distortion and possibly incur more exposed oxygen vacancies.

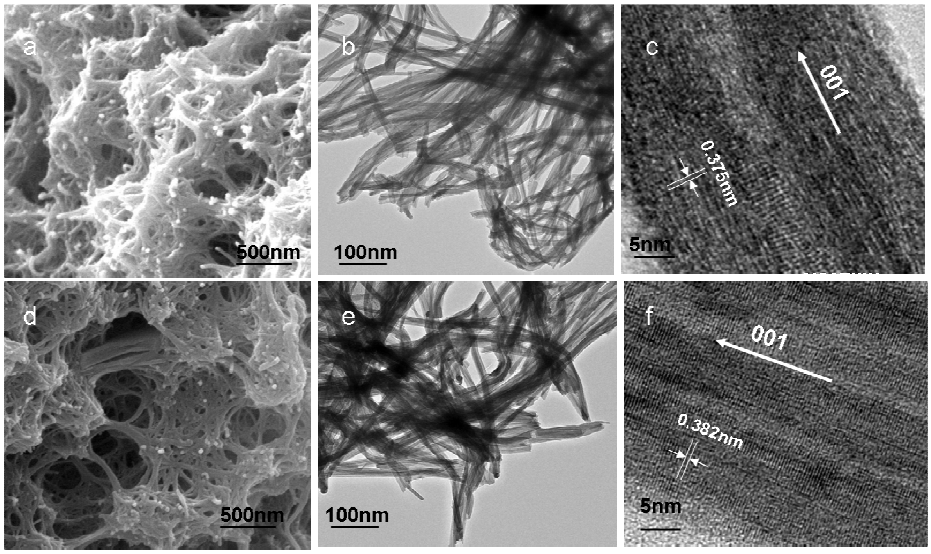

Fig.2. (a) SEM, (b) TEM and (c) HRTEM images of the pristine WO_3 nanowires. (d) SEM, (e) TEM and (f) HRTEM images of Li-doped WO_3 nanowires at a Li/W molar ratio of 0.05.

3.2. Oxygen vacancies, energy band gap and surface area of the pristine and Li-doped WO_3

A survey of the oxide-based electrocatalyst has revealed that the oxygen vacancies, energy band level, and surface textures of the electrode materials regulate their electrocatalytic performance.[30] In this part, the overall XPS spectra of Li-doped WO_3 presented in Fig.3a demonstrates the residence of W, O, and Li elements, the contents of which identify with the composition of hydrothermal mixture. The O1s XPS spectra of pristine and Li-doped WO_3 illustrated by Fig.3b, c features an asymmetrical peak. It has been deconvoluted into two separate peaks using Gaussian distributions,[31]

which are lattice O^{2-} at 530.30 eV, surface OH^{-} at 531.10 eV, respectively. The intensity of hydroxyl group is significantly higher for Li-doped WO_3 compared with the pristine. Although the OH^- resides as a minor oxygen vacancy, it is beneficial for inhibiting electron-hole recombination process, thereby improving the electron transmission efficiency, [32-33] further enchanting the electrocatalytic activities of WO_3. Moreover, the real ratios of Li/W in Li-doped WO_3 samples were measured by ICP-OES (see ESI, Table 1†).

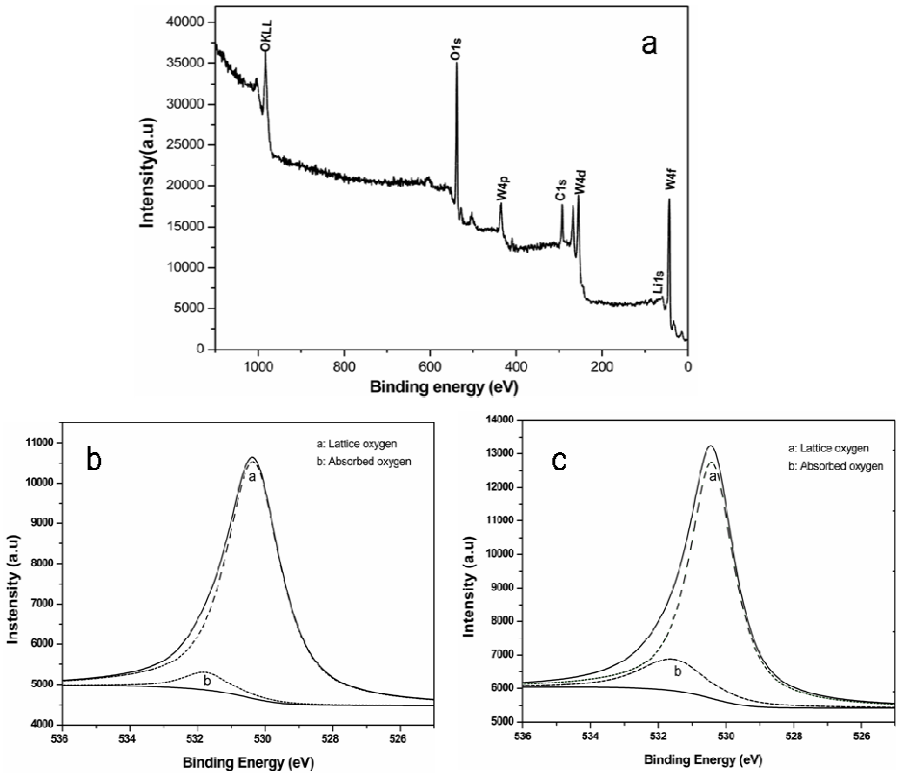

Fig.3. XPS spectra of (a) Li-doped WO_3 (Li/W = 0.05). XPS O1s spectra of (b) undoped and (c) doped WO_3.

The energy band level has been assessed via a conventional UV-vis spectroscopy. As illustrated in **Fig.4,** the maximum reflectance shifts to higher wavelength after Li doping**.** The band gap energy (E_g) of the semiconductor can be determined

accordingly:

$$\alpha hv = A(hv - E_g)^n \quad (1)$$

Where α is the absorption coefficient, hv is the incident photon energy, A is a constant, and n is either 2 or 1/2 for direct and indirect transitions, respectively.[34-35] It is known that WO_3 crystal is an indirect-gap semiconductor, thus a n value of 2 is assumed here. The band gap determined by the linear extrapolation presented in the inset are approximately 3.05, 2.88 eV for the pristine and Li-doped WO_3 (Li / W mole ratio of 0.05), respectively. The narrowing of Li-doped WO_3 energy band gap could be interpreted in the two mentioned aspects: (1) the local lattice distortion possibly change the electronic structure and carrier density of WO_3, which results in the improvement of its electrocatalytic activity.[14,17] (2) the oxygen vacancies incur defect band with a low energy.[29]

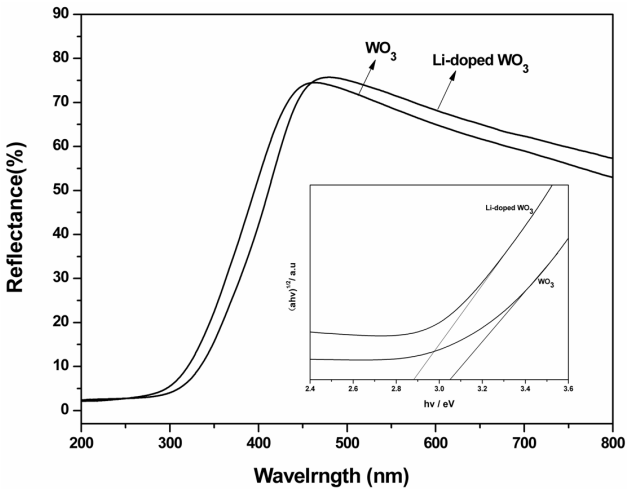

Fig.4. UV–vis reflectance spectra of undoped and Li-doped WO_3 (Li/W = 0.05). The inset is a plot of $(\alpha hv)^{1/2}$ as a function of hv for the undoped and doped WO_3 samples.

The active surface area of the nanoparticles that is also crucial to determining the electrocatalytic property was evaluated. The nitrogen adsorption–desorption isotherms

of the pristine and Li-doped WO_3 nanowires are shown in Fig.5. The BET surface areas of the pristine and Li-doped WO_3 nanowires were determined as 19.42 and 74.92 m^2 g^{-1}, respectively. As observed, WO_3 featured an enhanced surface area following doping with Li ions, indicative of the presence of a larger number of active sites that would be beneficial towards improving the electrocatalytic activity of the doped sample.

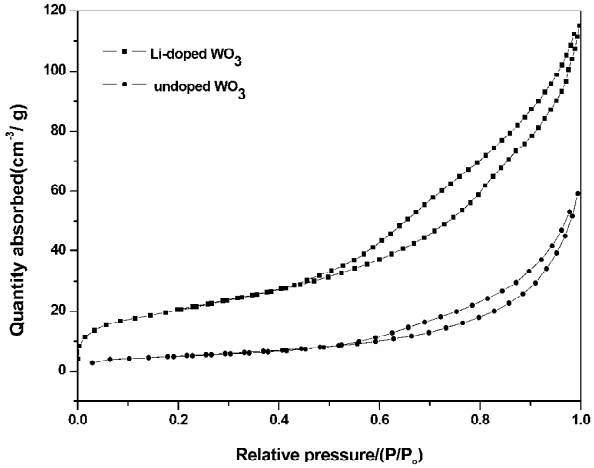

Fig.5. Nitrogen sorption isotherm curves of undoped WO_3 and Li-doped WO_3 (Li/W=0.05).

3.3. Electrocatalytic activity of the Li-doped WO_3 film-coated electrode

In this section, the electrocatalytic experimental parameters including the type of working electrode, the concentration of AA, the scan rate has been adopted to evaluate the electrocatalytic activity of the Li-doped WO_3 film-coated electrode. The cyclic voltammogram illustrated by Fig.6 left display an anodic peak (E_p) at 0.57 V (Curve a), 0.52 V (Curve c), 0.45 V (Curve b) for bare GCE, WO_3 film-coated electrode and Li-doped WO_3 film-coated electrode, respectively. Thus, there is a negative shift of 0.12 V of E_p on Li-doped WO_3 film-coated electrode. The negative shift of anodic peak position indicates Li-doped WO_3 film-coated electrode has excellent

electrocatalytic activity toward AA oxidation. Meanwhile, the Li doping amount has been optimized as a Li/W molar ratio of 0.05 since its anodic current is the maximum among those different doping ratio. (See Fig.6 right)

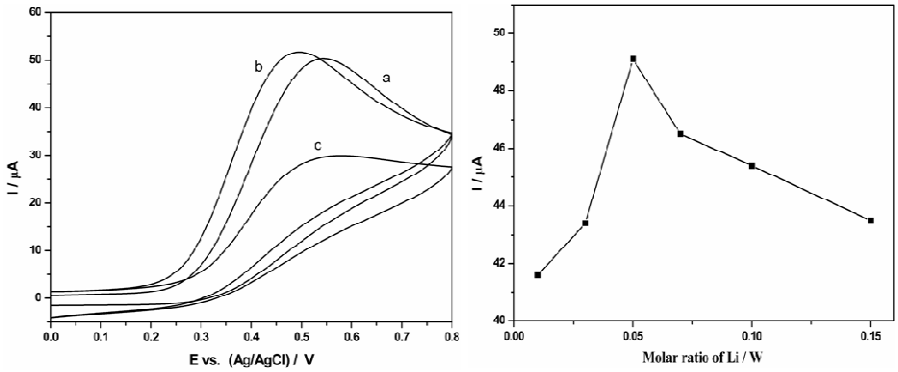

Fig.6. (Left) Cyclic voltammograms of 4 mmol L^{-1} AA adopting (a) bare GCE, (b) Li-doped WO_3, and (c) WO_3 electrode in 0.1 mol L^{-1} KCl solution. (Right) Variation of anodic current as a function of the Li/W molar ratios.

The Li-doped WO_3 film-coated electrode with the optimum doping amount is selected and the effect of AA concentration, scan rate on the anodic current has been assessed in Fig.7. Fig.7a shows the cyclic voltammograms of AA at varying concentrations in 0.1 mol L^{-1} KCl solution using the Li-doped WO_3 film-coated electrode. As observed, the oxidation peak current increased with increasing AA concentrations. The inset of Fig.7a shows a linear relationship between the anodic peak current and AA concentration in the range of 2–8 mmol L^{-1}, with a correlation coefficient of 0.998. At a fixed potential of 0.5 V the catalytic current observed was also linear dependent on the AA concentration in the range 0.01-4 mmol L^{-1} and the detection limit was 0.04 mmol L^{-1}. Furthermore, the as-prepared Li-doped WO_3 modified electrode is compared with other modified electrodes on aspects such as linear range and detection limit, which are shown in

Table 1, these information demonstrate the sensor behaves well with the wide linear range, low detection limit towards the oxidation AA.

The cyclic voltammograms of the Li-doped film-coated electrode at various scan

rates in the presence of 4 mmol L^{-1} AA in 0.1 mol L^{-1} KCl (Fig.7b) reveal that the catalytic effect of the Li-doped film-coated electrode appears at the higher scan rates because of the considerably higher catalytic reaction rate. Moreover, the catalytic oxidation peak potential shifts to more positive values with the increasing scan rates, indicative of a kinetics limitation in the reaction between the redox sites of Li-doped WO_3 film and AA. This result also proves that the electrochemical oxide reaction of AA is an irreversible process. The inset of Fig.7b shows the linear correlation between the anodic peak currents of AA and square-root of scan rates, indicative of a diffusion controlled electrode process.

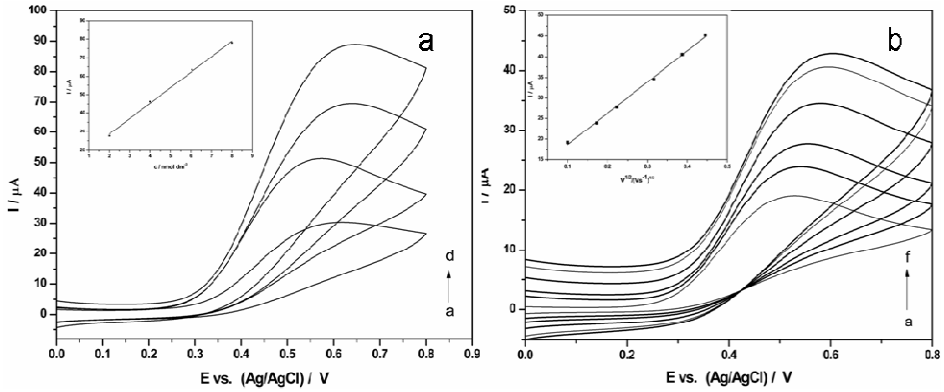

Fig.7. (Left) The concentrations of AA studied are (a)–(d) 2, 4, 6, and 8 mmol L^{-1}, respectively. (Right) The different potential scan rates of (a)–(f) 10, 30, 50, 70, 100 and 150 mV s^{-1}, respectively.

Table 1 Comparison of electrochemical parameters of the Li-doped WO_3 modified GCE with those of other modified electrodes reported in the literature

Modified electrode	Linear range (μmol L^{-1})	Detection limit (μmol L^{-1})	Reference
Li-doped Ta_2O_5 / GCE	5000-12000	—	17
Li doped Bi_2O_3/CNT/GCE	20-5000	50	36
Fe_3O_4@Au-s-Fc/GS-chitosan/GCE	6-350	5	37
MgO nanobelts /GCE	25-150	0.2	38
Nano-Cu/PSA III/GCE	0.3-730	0.15	39
Nano-CuO/GCE	0.1-3100	0.095	40
Nano-NiO/GCE	50-3500	860	41
Li-doped WO_3/GCE	2000-8000	40	This work

In order to explore the diffusion mechanism, two models have been adopted to determine the rate-limiting step of the process, which are the scan rate-normalized

current ($I/v^{1/2}$) as a function of scan rate (v), E_p as a function of logarithm of the scan rate (log v). The fitting results are illustrated by Fig.8. The shape of the curve in Fig.8a is typical of an electrochemical–chemical (EC) process.[42] To obtain information on the rate determining step, the following function involving E_p and logarithm of the scan rates (log v) for an irreversible diffusion-controlled process was assessed:[43]

$$\mathrm{Ep} = \left(\frac{2.303\mathrm{RT}}{2\alpha n_\alpha \mathrm{F}}\right)\log \nu + \mathrm{K} = \left(\frac{\mathrm{b}}{2}\right)\log \nu + \mathrm{K} \qquad (2)$$

Where K is a constant, α is the transfer coefficient, n_α is the number of electrons transferred, v is the scan rate, and b is the Tafel slope. Fig. 8b shows the variation of E_p with log v. The slope of the E_p–log v plot was determined as 0.067 and a Tafel slope of 0.134 were obtained. The value of $2.303RT/\alpha n_\alpha F$ is equivalent to the Tafel slope. The value of the transfer coefficient was then determined to be 0.429. Another method that is used for calculating the transfer coefficient (α) was also employed, using the following equation for an irreversible system[17, 44]

$$\Delta \mathrm{E_p} = \mathrm{E}_{\frac{\mathrm{p}}{2}} - \mathrm{E_p} = \frac{47.7}{\mathrm{n_a}\alpha} \qquad (3)$$

Where n_a is the number of electrons transferred during the electrochemical process.

The transfer coefficients obtained from the above fitting are in good agreement and indicate the electrocatalytic oxidation of AA is, an electrochemical–chemical (EC) process, simultaneously controlled by a diffusion of solution AA and cross-exchange through the Li-doped WO_3 film.

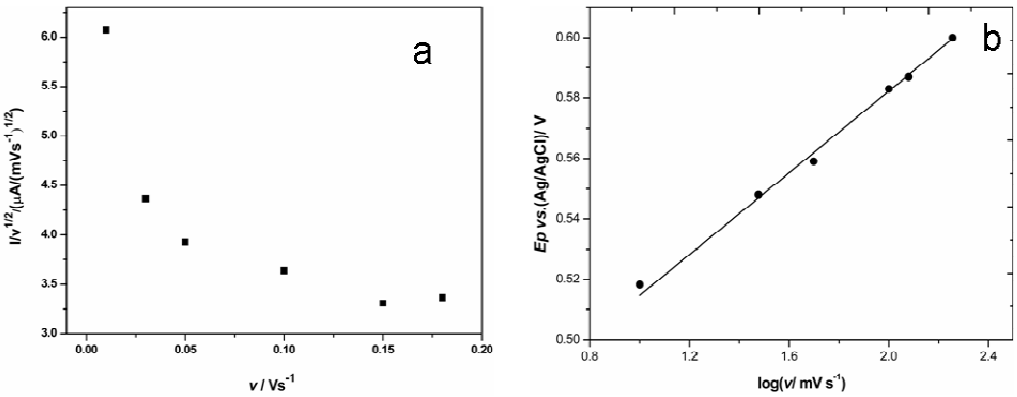

Fig.8. (Left) Plot of the anodic peak current ($I/v^{1/2}$) as a function of scan rate (ν). (Right) Dependence of the peak potential E_p on log ν for the oxidation of AA on Li-doped WO_3 film-coated electrode.

4. Conclusions

Creating the electron deficit by substituting some of the cations of the host oxide with cations having a lower valence is a versatile approach to tailor catalysts. Herein, the insertion of Li^+ into the WO_3 causes a lattice distortion, surface area enlargement and oxygen vacancy formation. The integrated effect of those structure determinants facilitates the oxidation of AA on the electrocatalyst surface, enhancing its electrocatalytic performance. The anodic peak potential of AA shifted from 0.57 V (versus Ag|AgCl) on a bare GCE to 0.45 V on the lithium-WO_3 film coated electrode. Despite the preliminary results demonstrate that Li-doped WO_3 film-coated electrode is promising electrochemical sensor for the detection of AA, the hydrothermal synthesis factors dominating the crystal structure and morphology, the advanced characterizations combined with quantum computation, the electrocatalytic experiments carried out in complex simulant bearing AA are in eager of in-depth investigations for the development of highly selective, sensitive and effective

electrochemical detector.

Acknowledgments

This work was financially supported by Institute of Nuclear Chemistry and Physics, China Academy of Engineering Physics.

References

1 L. Fernandez and H. Carrero, Electrochimica Acta, 2005, **50**, 1233.

2 N. F. Atta and M. F. El-Kady, Analytical Biochemistry, 2010, **400**, 78.

3 M.G. Hosseini, M. Faraji and M. M. Momeni, Thin Solid Films, 2011, **519**, 3457.

4 L. Zhang, Electrochimica Acta, 2007, **52**, 6969.

5 L. Zhang and S. J. Dong, Journal of Electroanalytical Chemistry, 2004, **568**, 189.

6 M. H. Pournaghi-Azar and H. Razmi-Nerbin, Journal of Electroanalytical Chemistry, 2000, **488**, 17.

7 E.Tsuji, A. Imanishi, K. Fukui and Y. Nakato, Electrochimica Acta, 2011, **56**, 2009.

8 J. Masud, M. T. Alam, Z. Awaludin, M. S. El-Deab, T. Okajima and T. Ohsaka, Journal of Power Sources, 2012, **220**, 399.

9 A. Moulahi, F. Sediri and N. Gharbi, Mater. Res. Bull, 2012, **47**, 667.

10 B. Klapste, J.Vondrak and J.Velicka J, Electrochimica Acta, 2002, **47**, 2365.

11 D. Das, P. K. Sen and K. Das, Electrochimica Acta, 2008, **54**, 289.

12 Y. J Feng and Y. H. Cui, Water Research, 2003, **37**, 2399.

13 J. Zhoo, N. S. Xu, S. Z. Deng, J. Chen and J. C. She, Chem. Phys. Lett, 2003, **382**, 433.

14 Q. Q. Du, X. F. Cao, B. Chi, J. Zhang, C. M. Zhang, T. Liu, X. J. Wang and Y. G. Su, Journal of Electroanalytical Chemistry, 2012, **681**, 139.

15 Y. H. Zhao, W. Y. Wang, Q. Y. Jia, Y. Gao, X. J. Wang and Y. G. Su, Journal of Inner Mongolia University, 2010, **41**, 307.

16 K. Senevirathne, V. Neburchilov, V. Alzate, R. Baker, R. Neagu, J. Zhang, S. Camp-bell and S. Ye, Journal of Power Sources, 2012, **220**, 1.

17 Y. H. Zhao, C. Y. Li, W. Zhao, Q. Q. Du, B. Chi, J. J. Sun, Z. L. Chai and X. J. Wang, Electrochimica Acta, 2013, 1**07**, 52.

18 X. J. Comini, C. Baratto, G. Faglia, M. Ferroni, A. Vomiero and G. Sberveglieri, Prog. Mater. Sci., 2009, **54**, 1

19 Y. Xie, F. C. Cheong, B. Varghese, Y. W. Zhu, R. Mahendiran and C. H. Sow, Sens. Actuators B, 2011, **151**, 320.

20 J. Yu, L. Qi, B. Cheng and X. Zhao, J. Hazard. Mater, 2008, **160**, 621.

21 L. E. Bevers, L. E. Hagedoorn and W. R. Hagen, Coord. Chem. Rev, 2009, **253**, 269.

22 S. Salmaoui, F. Sediri, N. Gharbi, C. Perruchot and M. Jouini, Electrochimica Acta, 2013, **108,** 634.

23 C. Santato, M.Odziemkowski, M. Ulmann and J. Augustynski, Journal of the American Chemical Society, 2001, **123,** 10639.

24 R.Solarska, A. Krolikowska and J. Augustynski, Angewandte Chemie International Editon, 2010, **49**, 7980.

25 J. Z. Su, X. J. Feng, J. D. Sloppy, L. J. Guo and C. A. Grimes, Nano Letters, 2011, **11** 203.

26 J. Rajeswari, P. S. Kishore, B. Viswanathan and T. K. Varadarajan, Nanorods Nanoscale Research Letters, 2007, **2**, 496.

27 S. R. Bathe and P. S. Patil, J. Phys. D: Appl. Phys, 2007, **40**, 74231.

28 G. F. Cai, X. L. Wang, D. Zhou, J. H. Zhang, Q. Q. Xiong, C. D. Guo and J. P. Tu, RSC Advances, 2013, **3**, 6896.

29 X. Xie, W. J. Mu, X. L. Li, H. Y. Wei, Y. Jian, Q. H. Yu, R. Zhang, K. Lv, H. Tang, S. Z. Luo, Electrochimica Acta, 2014, **134**, 201.

30 R. S. Mulliken, Journal of Chemical Physics, 1955, **23**, 1841.

31 E. A. Davis and N. F. Mott, Philos.Mag., 1970, **22** 903.

32 J. Tauc, A. Menth and D. L. Wood, Phys. Rev. Lett, 1970, **25**, 749.

33 S. Polarz, J. Strunk, V. Ischenko, M. W. E. Van den Berg, O. Hinrichsen, M. Muhler and M. Driess, Angewandte Chemie International Edition,2006, **45**, 2965.

34 H. T. Sun, C. Cantalini, L. Lozzi, M. Passacantando, S. Santucci and M. Pelino, Thin Solid Films, 1996, **287**, 258.

35 F. S. Manciu, J. L. Enriquez, W. G. Durrer, Y. Yun, C. V. Ramana and S. K. Gullapalli, Journal of Materials Research, 2010, **25,** 2401.

36 Z. Mohammed, T. W. Tan, Z. Zainal, A. H. Abdullah and J. K. Goh, International journal of electrochemical science,2010, **5**, 501.

37 M. L. Liu, Q. Chen, C. L. Lai, Y. Y. Zhang, J. H. Deng, H.T. Li and S. Z. Yao, / Biosensors and Bioelectronics, 2013, **48**, 75.

38 M. J. Li, W. L. Guo. H. J. Li, W. Dai and B. Yang, Sensors and Actuators B: Chemical, 2014, **204,** 629**.**

39 L. Zhang, W. J. Yuan and B. Q. Hou, J. Electroanal. Chem, 2013, **689**, 135.

40 C. X. Wang, J. Liu, X. Huang, H. H. Wang, Y. D. Zheng, L. Li, S. Y. Wang, S. Chen and Y. Jin, Applied Surface Science, 2014, **292**, 291**.**

41 C. Xia, X. Yanjun and W. Ning, Sensor. Actuat. B-Chem, 2011, **153**, 434.

42 A. P. Shpak, A. M. Korduban, M. M. Medvedskij and V. O. Kandyba, Journal of Electron Spectroscopy and Related Phenomena, 2007, **156**, 172.

43 G. Erdogdu and A. E. Karagozler, Talanta, 1997, **44**, 2011.

44 A. J. Bard and L. R. Faulkner, Electrochemical Methods: Fundamentals and Applications, 2nd ed, New York, 2011.